Stable Isotopes and Iron Oxide Mineral Products as Markers of Chemodenitrification.

ARTICLE *in* ENVIRONMENTAL SCIENCE AND TECHNOLOGY · FEBRUARY 2015

Impact Factor: 5.33 · DOI: 10.1021/es504862x · Source: PubMed

Environmental Science & Technology

Article

pubs.acs.org/est

Stable Isotopes and Iron Oxide Mineral Products as Markers of Chemodenitrification.

L. Camille Jones, Brian Peters, Juan S. Lezama Pacheco, Karen L. Casciotti, and Scott Fendorf*

Department of Earth System Sciences, Stanford University, 473 Via Ortega, Room 140, Stanford, California 94305, United States

Supporting Information

ABSTRACT: When oxygen is limiting in soils and sediments, microorganisms utilize nitrate (NO_3^-) in respiration—through the process of denitrification—leading to the production of dinitrogen (N_2) gas and trace amounts of nitrous (N_2O) and nitric (NO) oxides. A chemical pathway involving reaction of ferrous iron (Fe^{2+}) with nitrite (NO_2^-), an intermediate in the denitrification pathway, can also result in production of N_2O. We examine the chemical reduction of NO_2^- by Fe(II)—chemodenitrification—in anoxic batch incubations at neutral pH. Aqueous Fe^{2+} and NO_2^- reacted rapidly, producing N_2O and generating Fe(III) (hydr)oxide mineral products. Lepidocrotite and goethite, identified by synchrotron X-ray diffraction (XRD) and extended X-ray absorption fine structure (EXAFS) spectroscopy, were produced from initially aqueous reactants, with two-line ferrihydrite increasing in abundance later in the reaction sequence. Based on the similarity of apparent rate constants with different mineral catalysts, we propose that the chemodenitrification rate is insensitive to the type of Fe(III) (hydr)oxide. With stable isotope measurements, we reveal a narrow range of isotopic fractionation during NO_2^- reduction to N_2O. The location of N isotopes in the linear N_2O molecule, known as site preference, was also constrained to a signature range. The coexistence of Fe(III) (hydr)oxide, characteristic ^{15}N and ^{18}O fractionation, and N_2O site preference may be used in combination to qualitatively distinguish between abiotic and biogenically emitted N_2O—a finding important for determining N_2O sources in natural systems.

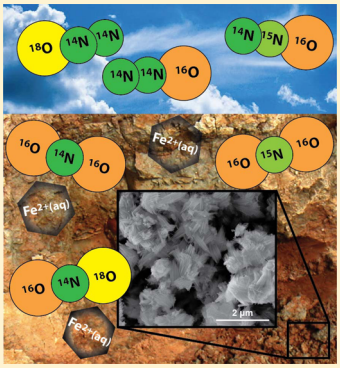

INTRODUCTION

Nitrous oxide (N_2O) is more than 200 times more effective at absorbing long-wave radiation than carbon dioxide (CO_2), making it a powerful greenhouse gas (GHG).[1] Because of its long residence time in the atmosphere, it has approximately 300 times the global warming potential of CO_2 on a time scale of 100 years.[1] Atmospheric N_2O is also the primary source of ozone-depleting NO_x (NO and NO_2) to the stratosphere.[2]

Natural production of N_2O has been attributed primarily to microbial processes in soils and aquatic environments, including denitrification—the biological reduction of nitrate (NO_3^-) or nitrite (NO_2^-) to gaseous nitric oxide (NO), N_2O, and eventually dinitrogen (N_2).[3−5] In addition to being linked to N_2O production, NO_2^- and NO_3^- are water contaminants due to their toxicity and connection to eutrophication.[6,7] Even though denitrifying soil microorganisms are a natural source of N_2O, chemical denitrification also contributes to N_2O emission.[8,9]

Chemical denitrification, or chemodenitrification, is the abiotic reduction of NO_x^- by ferrous iron (Fe^{2+}), producing NO and N_2O gases along with Fe(III) hydroxides, oxyhydroxides, and oxides (hereafter collectively referred to as Fe(III) oxides) as byproducts. In Reaction 1, ferric oxyhydroxide is depicted as a product resulting from Fe(II) oxidation and NO_2^- reduction.

$$4Fe^{2+} + 2NO_2^- + 5H_2O \rightarrow 4FeOOH + N_2O + 6H^+$$
$$\Delta G^\circ = -128.5\ \text{kJ mol}^{-1} \quad (1)$$

First described in 1966, this reaction has now been characterized over a range of conditions including various Fe(III) (hydr)oxide mineral catalysts.[10−15] The reaction is initiated by contact between Fe^{2+} and NO_2^-, followed by a series of one-electron transfer steps and finally dimerization to produce N_2O.[16,17] The ideal condition for chemodenitrification is a fluctuating redox zone where Fe^{2+}, which occurs in anaerobic conditions, and NO_2^- and Fe(III) oxides, which dominate in oxygenated regions, can interact.[8,18,19] Periodically flooded soils, soil aggregates, and plant rhizospheres are a few examples where relevant redox boundaries and fluctuations can occur.

Resolving chemical versus biological denitrification, especially in natural settings, is critical for characterizing environmental controls on soil N_2O emission.[19−21] The objective of the present study is to evaluate mineral and isotope markers of chemodenitrification and the conditions that affect them. For the first time, Fe(III) oxides formed from aqueous Fe^{2+} oxidized by NO_2^- have been characterized using synchrotron-based spectroscopy and evaluated for their kinetic effect on the reaction. Stable isotopic analysis of the N_2O can be used to distinguish pathways of N_2O production in the environment.[22−28] Accordingly, here we characterize the effects of

Received: October 4, 2014
Revised: February 15, 2015
Accepted: February 16, 2015
Published: February 16, 2015

DOI: 10.1021/es504862x
Environ. Sci. Technol. 2015, 49, 3444−3452

stable isotope fractionation on the isotopic compositions of NO_2^- and N_2O involved in chemodenitrification. Connecting the rates, Fe cycle, and isotope effects of chemodenitrification may thus lead to identifying causal mechanisms for N_2O production and will help target solutions to reduce groundwater pollution and GHG emission.

MATERIALS AND METHODS

Chemodenitrification Incubations. Batch incubations were used to determine the rate of NO_2^- reduction by Fe^{2+} and production of N_2O. The matrix solution used in all reactions was 10 mM NaCl, 30 mM piperazine-N,Ǹ-bis(2-ethanesulfonic acid) (PIPES) buffer adjusted to pH 7.0, and deoxygenated distilled deionized (DDI) water. Ferrous iron stock solution was prepared from reagent grade $FeCl_2{\cdot}4H_2O$ and deoxygenated DDI water. Nitrite stock solution was prepared from reagent grade $NaNO_2$ and deoxygenated DDI water. All reagents and experiments were mixed and sampled in an anaerobic glovebox with an N_2 (95%) H_2 (5%) atmosphere (Coy Laboratory Products).

Triplicate batch incubation experiments included 12 mL of buffer solution with Fe^{2+} and NO_2^- (from anoxic stock solutions) reacting in acid-washed 20 mL sealed glass serum bottles. All batch incubations were prepared in an anaerobic glovebox to ensure the exclusion of O_2. Incubations were shaken in a dark incubator at 26 ± 1 °C and reacted for 3 days or until no further change in Fe^{2+} or N_2O was observed. Control incubations contained buffer with NO_2^- or Fe^{2+} alone and did not result in any loss of those solutes. Three reaction conditions were examined:

"excess NO_2^-": 40 mM NO_2^- reacted with 5 mM Fe^{2+},
"equimolar": 10 mM NO_2^- reacted with 10 mM Fe^{2+},
"excess Fe": 2.5 mM NO_2^- reacted with 10 mM Fe^{2+}

All experiments began as homogeneous aqueous reactions but quickly resulted in production of an Fe(III) (hydr)oxide precipitate, shifting NO_2^- reduction to a heterogeneous reaction. To examine an initially heterogeneous reduction of NO_2^- by Fe(II)-adsorbed on Fe(III) oxides, batch incubations were also started by adding spikes of Fe^{2+} and NO_2^- to incubations that contained Fe(III) (hydr)oxide minerals formed from homogeneous starting conditions containing Fe^{2+} and NO_2^-.

Aqueous and Gas Phase Analyses. Aqueous and adsorbed Fe^{2+} were measured with ferrozine (3-(2-pyridyl)-5,6-diphenyl-1,2,4-triazine-*p*,*p*′-disulfonic acid).[29] In the glovebox, ferrozine was added to each aqueous sample before the ferrozine-complexed solution was filtered (0.2 μm PES filters). Therefore, Fe^{2+} reported here included the sum of aqueous and Fe^{2+} desorbed from the mineral surface. Absorbance at 562 nm was measured on a UV/vis spectrophotometer (Shimadzu UV-1601).

Nitrite was measured colorimetrically after samples were oxidized and filtered to stop the reaction, according to the pink-azo dye method.[30] Samples were analyzed in duplicate using a Gilson 222XL Liquid Handler connected to an Ultraspec 2100 Pro UV/vis Spectrophotometer (Amersham Biosciences).

Nitrous oxide was measured on a gas chromatograph (GC) equipped with electron capture detector (Shimadzu GC-2014). Two mL gas samples were withdrawn from incubation bottles using gastight syringes, transferred immediately to He-evacuated gastight vials, and 3−4 mL were injected in to the GC with gastight syringes. Nitrous oxide standards were 0.36, 1.0, 1.69, and 10 ppm. Methods for determining Fe^{2+} and NO_2^- were standardized using calibration curves generated from solutions of known Fe^{2+} and NO_2^- concentration.

To describe the kinetics of chemodenitrification in our batch incubations, we assumed reaction 1 is operative. We used initial rates (0−24 h) so that we could assume back reactions were not affecting the reaction rate and only forward reactions (i.e., Fe^{2+} oxidation and NO_2^- reduction) were involved. The overall apparent kinetic rate law is

$$d[NO_2^-]/dt = -k_1[NO_2^-][Fe^{2+}] \quad (2)$$

Apparent first order rate expressions were described by the rate constant k_{obs} in the overall rate equations by employing excess of a single reactant such that

$$d[Fe^{2+}]/dt = -k_{obs1}[Fe^{2+}] \quad (3)$$

$$d[NO_2^-]/dt = -k_{obs2}[NO_2^-] \quad (4)$$

where k_{obs1} is the apparent rate constant for loss of Fe^{2+} and k_{obs2} is the apparent rate constant for loss of NO_2^-. Rates and rate constants for the initial reaction were determined in batch incubations with at least four concentration and time data points. Specifically, rate coefficients were determined from a first order model with respect to Fe^{2+} or NO_2^-, using the slope of the best fit line to concentration data plotted as $\ln[Fe^{2+}]$ versus time or $\ln[NO_2^-]$ versus time for 0, 6, 12, and 24 h.

Solid Phase Analyses. Solid phases were collected from the incubations by vacuum filtration inside the anaerobic N_2/H_2 atmosphere glovebox. Solids were filtered on to 0.1 μm filters (VCTP Millipore Isopore), rinsed with deoxygenated DDI water followed by dilute ethanol, and dried in the glovebox. Solids from excess NO_2^- and equimolar homogeneous conditions were analyzed by synchrotron-based techniques. X-ray diffraction (XRD) measurements were conducted on beamline 11−3 at the Stanford Synchrotron Radiation Lightsource (SSRL). Quantitative identification of Fe oxide phases was achieved by extended X-ray absorption fine structure (EXAFS) spectroscopy on beamlines 4−1 and 11−2 at SSRL. Technical aspects of synchrotron-based analyses are described in the Supporting Information (SI).

We obtained scanning electron microscope (SEM) images of the solids from the equimolar experimental condition. Imaging was done at 10.00 kV at the Stanford Nanocharacterization Laboratory on the FEI Magellan 400 XHR SEM. Samples were prepared by drop-casting mineral suspensions on aluminum holders.

Stable Isotope Methods. N and O isotopic ratios of NO_2^- were determined using the azide method.[31] Samples were dispensed into duplicate gastight serum vials and purged with N_2 gas, removing any N_2O in the sample produced during the reaction prior to the addition of sodium azide. The N_2O produced from NO_2^- during the azide step was then analyzed on a Finnigan Delta^{PLUS} XP isotope ratio mass spectrometer. Nitrite isotope standards RSIL N23, N7373, and N10219 were prepared and run in parallel with samples.[32] Values for $\delta^{15}N_{NO_2^-}$ and $\delta^{18}O_{NO_2^-}$ are reported as delta values in units of per mil (‰): $\delta = (R_{sample}/R_{standard} - 1) \times 1000$, where R_{sample} and $R_{standard}$ are the $^{15}N/^{14}N$ (or $^{18}O/^{16}O$) of the sample and standard, respectively. The standard used for reporting $^{15}N/^{14}N$ ratios is atmospheric N_2 ($^{15}R_{air\ N2}$ = 0.0036765) and for $^{18}O/^{16}O$ it is Vienna Standard Mean Ocean Water (VSMOW, $^{18}R_{VSMOW}$ = 0.0020052). The precision of these measurements

DOI: 10.1021/es504862x
Environ. Sci. Technol. 2015, 49, 3444−3452

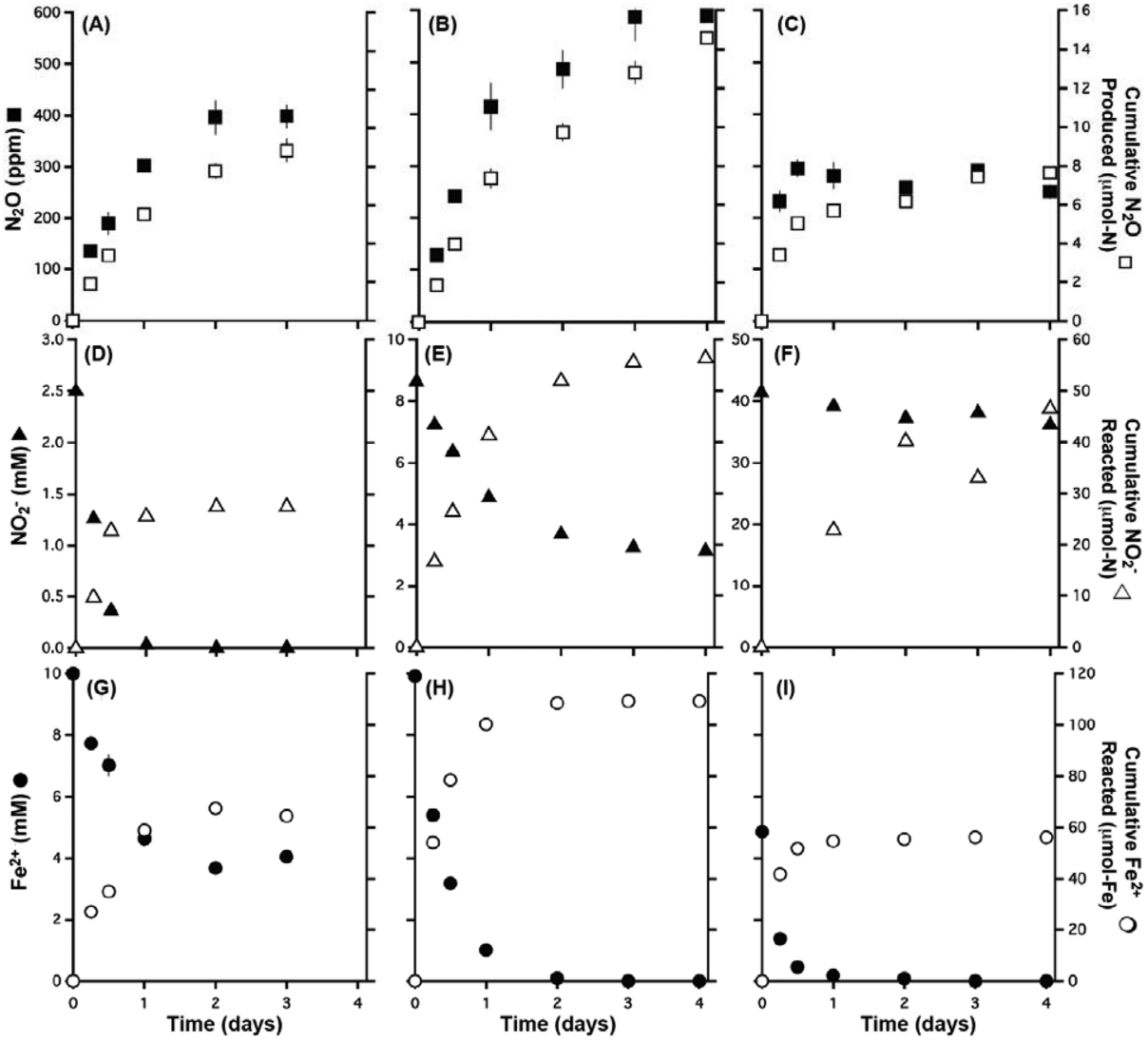

Figure 1. Appearance of N_2O (A, B, C), loss of NO_2^- (D, E, F), loss of Fe^{2+} (G, H, I) over time, including cumulative N_2O produced, NO_2^- reacted, and Fe^{2+} reacted. The excess Fe condition (2.5 mM NO_2^-, 10 mM Fe^{2+}) is panels A, D, and G. The equimolar condition (10 mM NO_2^-, 10 mM Fe^{2+}) is panels B, E, and H. The excess NO_2^- condition (40 mM NO_2^-, 5 mM Fe^{2+}) is panels C, F, and I. Black symbols are bulk concentrations and open symbols are reacted quantities per vial. Note the difference in *y*-axis scales for NO_2^- measurements. Error bars are the standard deviation of triplicate experiments and they are smaller than most markers.

is 0.2‰ for $\delta^{15}N_{NO2}$ and 0.5‰ for $\delta^{18}O_{NO2}$, based on replicate standard injections.[31]

Determination of the isotopic composition of N_2O involved a standard method for bulk isotopic compositions, $\delta^{15}N^{bulk}$ and $\delta^{18}O$, as well as the site-specific $\delta^{15}N$ measurements of the central (N^{α}) and outer (N^{β}) atoms in the linear N_2O molecule.[33] Site preference (SP) was determined from the difference in $\delta^{15}N$ between the central and outer positions (SP (‰) = $\delta^{15}N^{\alpha}$ - $\delta^{15}N^{\beta}$). Sample analyses were calibrated against reference gas injections.[34] Sample-size dependencies of the instrument due to nonlinear effects were corrected by analyzing reference N_2O gas in varying amounts.[33] These corrections ranged from 0.1‰ to 3.9‰ for $\delta^{15}N^{bulk}$, 0.1‰ to 0.8‰ for $\delta^{18}O$, and 0.1‰ to 7.9‰ for SP.[33] Precision for replicate analyses of a laboratory N_2O working gas is 0.3 ‰ for $\delta^{15}N^{bulk}$, 0.5‰ for $\delta^{18}O$, and 1‰ for SP.[33] Accuracy for these measurements was determined through parallel analyses of atmospheric N_2O, which has an accepted $\delta^{15}N^{bulk}$ of 7.0 ± 0.6‰, $\delta^{18}O$ of 43.7 ± 0.9‰, and SP of 18.7 ± 2.2‰.[22] A recent intercalibration for N_2O isotopes conducted in our lab produced results comparable to the Tokyo Institute of Technology.[35]

RESULTS

Chemodenitrification Kinetics. Rapid N_2O generation from NO_2^- reduction coupled with Fe^{2+} oxidation was observed in all anaerobic batch incubations. All reactions had at least two reaction phases, which we characterize as a rapid initial phase followed by a slower phase after 24 h. Initial rates of removal of Fe^{2+} from solution by oxidation and, potentially, sorption were 211 ± 0.26 μM h^{-1} for the excess Fe (2.5 mM NO_2^- reacted with 10 mM Fe^{2+}) condition (Figure 1A, D, G), 349 ± 0.15 μM h^{-1} for the equimolar (10 mM NO_2^- reacted with 10 mM Fe^{2+}) condition (Figure 1B, E, H), and 172 ± 0.08 μM h^{-1} for the excess NO_2^- (40 mM NO_2^- reacted with 5 mM Fe^{2+}) condition (Figure 1C, F, I). Previous laboratory-based work reported N_2O production, Fe^{2+} oxidation rates (ranging from 134 μM h^{-1} to 301 μM h^{-1}), and reaction stoichiometry

DOI: 10.1021/es504862x
Environ. Sci. Technol. 2015, 49, 3444−3452

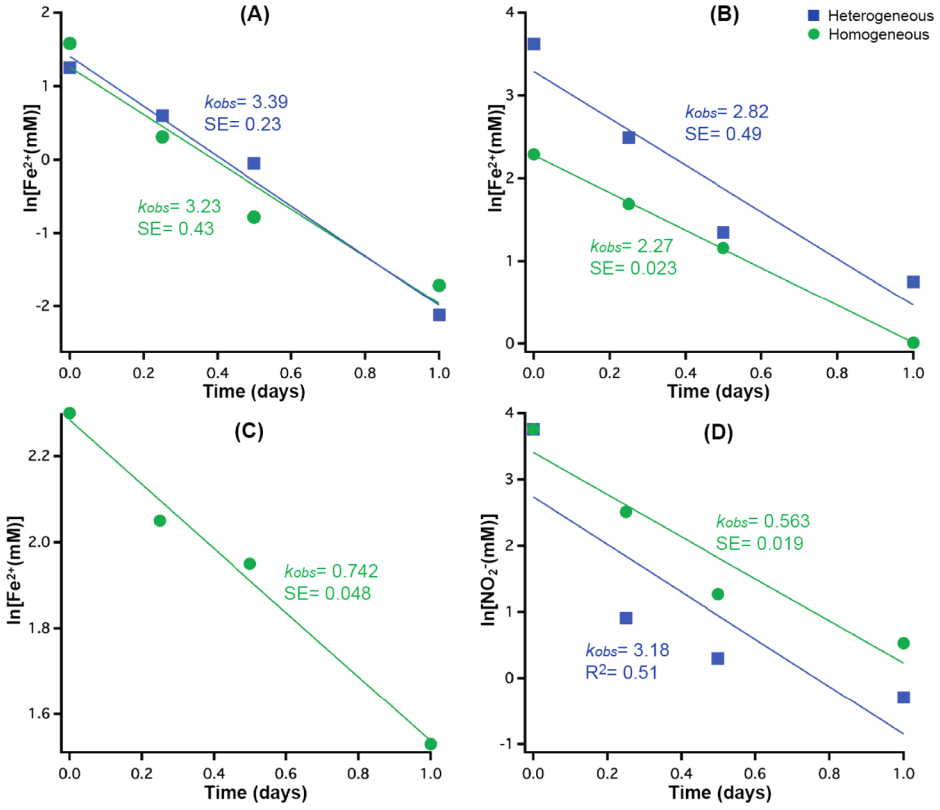

Figure 2. Disappearance of Fe^{2+} and NO_2^- from solution in heterogeneous (squares) and initially homogeneous (circles) batch incubations plotted with the apparent first order kinetic model. Panel (A) is the excess NO_2^- condition (40 mM NO_2^-, 5 mM Fe^{2+}); panel (C) is the excess Fe condition (2.5 mM NO_2^-, 10 mM Fe^{2+}), for which no mineral-catalyzed experiment was done, and panels (B) and (D) are the equimolar condition (10 mM NO_2^-, 10 mM Fe^{2+}). Data from 0 to 24 h were used to avoid back- and secondary-reactions. Rate constants and standard error (SE) values are shown on the plots.

(2 Fe^{2+} to 1 NO_2^-) consistent with our results.[11,12,14,15,17,36] However, on a molar basis, N_2O produced was only approximately 15−40% of the NO_2^- consumed (Figure 1), which shows that additional N-containing products were generated. The yield of N_2O from NO_2^- was highest under excess Fe^{2+} conditions (0.38 mol N_2O−N produced/mol NO_2^- consumed), intermediate under equimolar conditions (0.26 mol N_2O−N produced/mol NO_2^- consumed) and lowest under excess NO_2^- conditions (0.16 mol N_2O−N produced/mol NO_2^- consumed).

The catalytic effect of Fe (hydr)oxide minerals, which was demonstrated in previous studies, was confirmed by our experiments.[11,12,37] Past studies examined Fe(III) (hydr)oxide and carbonate minerals (e.g., green rust, magnetite, hydrous ferric oxide, and siderite) as catalysts for chemodenitrification.[12,15,38,39] Here, we considered the influence of the Fe(III) (hydr)oxide generated during chemodenitrification on the rate of Fe^{2+} induced reduction of NO_2^-.

Although the NO_2^- reaction with Fe^{2+} was initially homogeneous, it became heterogeneous almost immediately, as aqueous Fe^{2+} was rapidly transformed into Fe(III) that hydrolyzed to from ferric (hydr)oxide. Examination of the reaction kinetics illustrates that chemodenitrification rates were similar in experiments that started with Fe(III) (hydr)oxide to those starting with homogeneous aqueous reactants (Figure 2). We examined the initial reaction phase (0 to 24 h) because it deviated from apparent first order after 24 h. Kinetic calculations on loss of NO_2^- were performed only on the equimolar condition because other conditions had either too few NO_2^- measurements or too low concentration of NO_2^- between 0 and 24 h. Our results confirm previous work with respect to reaction rates, but a critical outstanding question is whether the Fe mineralogy influences the rate of chemodenitrification.

Iron Mineralogy. We observed the formation of various Fe(III) (hydr)oxide minerals during chemodenitrification. On a macroscopic level, an orange-yellow mineral suspension appeared within hours of starting the incubations. The color was similar to what has been previously reported, except that we did not observe green or black pigmentation, indicative of green rust and magnetite.[11,15,17] Indeed, neither green rust nor magnetite was detected by XRD. On the basis of morphological features observed by SEM (not shown), several minerals were present within the solid-phase assemblage.

Two-line ferrihydrite, lepidocrocite (γ-FeO(OH)), and goethite (α-FeO(OH)) were identified using XRD and EXAFS spectroscopy in solids from equimolar and excess NO_2^- incubations (SI Figures 1 and 2). X-ray diffraction peaks changed over time for mineral products collected at 6, 24, and 48 h, indicating an evolving mineral assemblage (SI Figure 1). Linear combination fitting of EXAFS spectra also showed a change in Fe(III) (hydr)oxide minerals between 6, 24, and 48 h time points (Table 1, SI Figure 2). The equimolar experiments maintained a nearly equal proportion of ferrihydrite, lepidocrocite, and goethite after 48 h of reaction. The excess NO_2^- experiments had less goethite throughout but produced relatively more goethite and ferrihydrite over time. Overall,

DOI: 10.1021/es504862x
Environ. Sci. Technol. 2015, 49, 3444−3452

Table 1. Iron(III) Oxide Mineral Fractions Resulting from Reaction of NO_2^- with Fe^{2+} after 6, 24, and 48 h of Reaction, Determined by Linear Combination EXAFS Spectral Fitting[a]

equimolar condition (10 mM NO_2^- 10 mM Fe^{2+})			
time (h)	ferrihydrite	lepidocrocite	goethite
6	0.40	0.28	0.32
24	0.39	0.27	0.34
48	0.33	0.30	0.37
excess NO_2^- condition (40 mM NO_2^- 5 mM Fe^{2+})			
time (h)	ferrihydrite	lepidocrocite	goethite
6	0.6	0.58	0.06
24	0.42	0.50	0.07
48	0.41	0.49	0.10

[a]Starting reactant concentrations in homogenous experiments are labeled at top. Error is ±5%.

chemodenitrification generated a variety of Fe(III) (hydr)oxide minerals.

Stable Isotopes. Trends in isotopic fractionation can provide useful information about mechanisms of N_2O production. We report measurements of $\delta^{15}N$ and $\delta^{18}O$ in NO_2^- and N_2O during the course of the excess Fe and equimolar experiments to establish an isotopic fingerprint for abiotic N_2O production from NO_2^-. In the excess Fe experiment, $\delta^{15}N$ and $\delta^{18}O$ of NO_2^- increased until NO_2^- was completely consumed after 1 day, following a trend expected for normal kinetic isotope fractionation (Figure 3A; SI Figure 3). $\delta^{15}N$ and $\delta^{18}O$ of N_2O also increased from −14.0 ± 0.2‰ to 0.2 ± 2.2‰ and 26.1 ± 0.2‰ to 36.5 ± 2.3‰, respectively (Figure 3B). The N_2O SP remained constant at around 10‰ (Figure 3B). There was an offset in $\delta^{15}N$ between NO_2^- and N_2O ($\Delta^{15}N = \delta^{15}N_{NO_2^-} - \delta^{15}N_{N_2O}$) of 28.1 ± 11.0‰ and $\delta^{18}O$ offset ($\Delta^{18}O = \delta^{18}O_{NO_2^-} - \delta^{18}O_{N_2O}$) of −4.4 ± 6.9‰ for the excess Fe experiment, both of which increased over time (Figure 3**C**). It was also observed that ^{18}O enrichment was weaker than ^{15}N enrichment for both NO_2^- and N_2O in the excess Fe experiment, with changes in $\delta^{18}O$ approximately 75 ± 10% of changes in $\delta^{15}N$ (SI Figure 3; SI Table 1).

In the equimolar experiment, $\delta^{15}N$ of NO_2^- increased until NO_2^- reduction ceased after 2 days (Figure 3**D**), at which time the reaction became Fe^{2+}-limited (Figure 1**H**) with NO_2^- remaining in solution (Figure 1**E**). $\delta^{18}O$ of NO_2^- increased during the first 24 h, decreased until 72 h, and then leveled off. $\delta^{15}N$ of N_2O increased from −16.8 ± 0.7‰ to −11.8 ± 0.1‰ during the first 24 h, and subsequently remained constant (Figure 3**E**). $\delta^{18}O$ of N_2O increased from 24.3 ± 1.0‰ to 28.8 ± 0.3‰ during the first 24 h, and remained constant (Figure 3**E**). Site preference values increased to 22‰ at the beginning of the experiment, but reached a steady value near 16‰ (Figure 3E).

The nonlinear behavior of $\delta^{18}O_{NO_2^-}$ in the equimolar experiment most likely reflects O atom exchange between NO_2^- and H_2O (Figure 3D).[40] After the first 24 h of the equimolar experiment, NO_2^- consumption slowed considerably but $\delta^{18}O_{NO_2^-}$ continued to change even after the NO_2^- was no longer being consumed. At this point, the abiotic exchange is expected to be the dominant process controlling $\delta^{18}O_{NO_2^-}$. Based on the temperature, pH, and $\delta^{18}O_{H_2O}$ of the experiment, we estimate the $\delta^{18}O_{NO_2^-}$ at equilibrium with water to be 0.3 ± 0.5‰ (see SI for details). This is indistinguishable from the final $\delta^{18}O_{NO_2^-}$ measured at the end of the experiment (−0.4 ± 0.2‰).

Overall, the changes in $\delta^{15}N^{bulk}$ and $\delta^{18}O$ of N_2O were smaller in the equimolar experiment compared to the excess Fe experiment, although the observed ^{18}O enrichment of N_2O was again weaker than enrichment of $^{15}N^{bulk}$, with changes in $\delta^{18}O$ approximately 70 ± 10% of changes in $\delta^{15}N^{bulk}$ (Figure 3E). The late decrease in $\delta^{18}O_{NO_2^-}$ (Figure 3D) clearly deviates from observations in the excess Fe experiment (Figure 3A). However, the early time points showed similar trends and offsets in isotopic compositions of N_2O and NO_2^- as compared to the excess Fe experiment, with $\delta^{15}N_{N_2O}$ lower than $\delta^{15}N_{NO_2^-}$ ($\Delta^{15}N = 27 \pm 4.5$‰) and $\delta^{18}O_{N_2O}$ higher than $\delta^{18}O_{NO_2^-}$ ($\Delta^{18}O = -19.3 \pm 8.2$‰) (Figure 3F). These isotopic offsets reflect isotopic fractionation during abiotic N_2O production from NO_2^-, but they represent the substrate in a closed system in the case of NO_2^- and an accumulating product in the case of N_2O. It is not expected, therefore, that N_2O shows the same change in $\delta^{15}N$ or $\delta^{18}O$ as NO_2^-, and their offsets predictably change over time (Figure 3C, F).

Raleigh equations were also used to calculate a kinetic nitrogen isotope effect ($^{15}\varepsilon$) for NO_2^- reduction. Here $^{15}\varepsilon$ is defined as $(^{15}\alpha - 1) \times 1000$ and $^{15}\alpha = {}^{15}R_s/{}^{15}R_{pi}$, which is >1 for a normal kinetic isotope effect leading to positive ε values. We find $^{15}\varepsilon$ values of 12.9 ± 3.0‰ for NO_2^- reduction in the excess Fe experiment and 18.1 ± 1.7‰ for NO_2^- reduction in the equimolar experiment (SI Figure 3A). An oxygen isotope effect ($^{18}\varepsilon$; defined as for ^{15}N, but with $^{18}\alpha = {}^{18}R_s/{}^{18}R_{pi}$) for NO_2^- reduction of 9.8 ± 1.8‰ for the excess Fe experiment also fits with the early time points of the equimolar experiment (SI Figure 3B). These observations of SP, $\Delta^{15}N$, $\Delta^{18}O$ and the fractionation of N isotopes relative to O isotopes may aid in distinguishing chemodenitrification from other sources of N_2O, as discussed below.

DISCUSSION

Iron oxide minerals formed during the onset of chemodenitrification may induce a feedback to both the N and Fe cycles, influencing N_2O production and redox-active metal and metalloid cycles. The chemodenitrification reaction sequence:

$$Fe^{2+} + NO_2^- + H_2O \rightarrow FeOOH + NO + H^+ \quad (7)$$

$$NO + Fe^{2+} + 2H_2O \rightarrow NO^- + FeOOH + 3H^+ \quad (8)$$

$$2NO^- + 2H^+ \rightarrow N_2O + H_2O \quad (9)$$

suggests that there may be accumulation of the NO intermediate. Indeed, NO has recently been detected in chemodenitrification.[11] The isotopic offsets between NO_2^- and N_2O reflect the number of reaction steps between the two species, individual isotopic fractionation factors for each step, and accumulation of intermediates. Indeed, much of the NO_2^- consumed was not accounted for as N_2O and likely accumulated as NO, which would contribute to the large (27−29‰) $\delta^{15}N$ difference between NO_2^- and N_2O, especially given that the isotope effect for NO_2^- reduction alone was found to be much smaller (13−18‰). Based on mass balance considerations, N_2O appears to be depleted in ^{15}N relative to the removed NO_2^-, meaning a pool of relatively high $\delta^{15}N$

DOI: 10.1021/es504862x
Environ. Sci. Technol. 2015, 49, 3444−3452

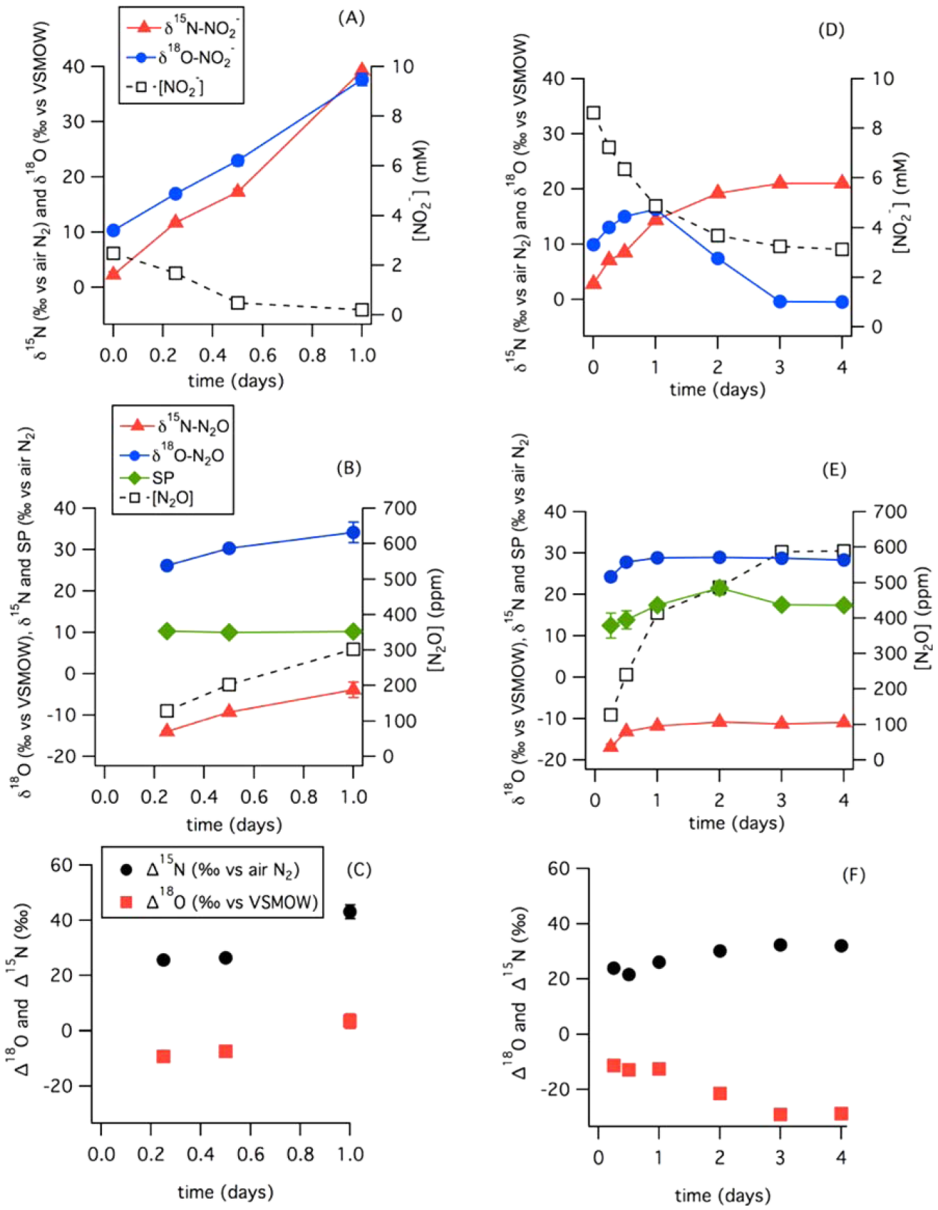

Figure 3. Changes in concentration, $\delta^{18}O$, and $\delta^{15}N$ of NO_2^- over time (A, D). Changes in concentration, $\delta^{18}O$, $\delta^{15}N$, and SP of N_2O over time (B, E). Changes in the $\delta^{15}N$ and $\delta^{18}O$ offsets ($\Delta^{15}N$ and $\Delta^{18}O$, respectively) between NO_2^- and N_2O (C, F). Panels on the left (A, B, and C) are for the 2.5 mM NO_2^- with 10 mM Fe^{2+} (excess Fe) experiment, and panels on the right (C, D, and E) are for the 10 mM NO_2^- with 10 mM Fe^{2+} (equimolar) experiment.

material accumulates, most likely as NO or N_2. A larger than expected $\delta^{15}N$ offset between NO_2^- and N_2O could result if NO_2^- is reduced to N_2, during the course of the reaction. In this case, heavy N would have to be preferentially transferred to the N_2 pool, though, which seems unlikely given that it is more reduced than NO and N_2O. It is easier to explain the offset with a heavy pool of N accumulating as NO, with ^{14}N being preferentially reacted to N_2O. The N isotopic fractionation during abiotic NO_2^- reduction observed here is similar to that occurring during bacterial NO_2^- reduction.[41] Likewise, a branching isotope effect, as observed for microbial NO_2^- reduction, most likely contributes to the ^{18}O enrichment in N_2O relative to NO_2^- (negative $\Delta^{18}O$) given that NO_2^- reduction preferentially removes ^{16}O from the N oxides.[32]

Previous studies have suggested that chemodenitrification requires a mineral catalyst.[16,36,39,42] Although our experiments may have been initially accelerated with addition of Fe(III) oxide (Figure 2), we find that the reaction proceeds without an initial solid phase. Moreover, even when the reaction starts homogeneously, Fe(III) oxides are formed immediately, giving the reaction a positive feedback and providing an autocatalytic pathway. This positive feedback is likely to be involved in a range of environments at near neutral pH and high NO_2^- and Fe^{2+} concentrations.

We observed formation of lepidocrocite, goethite, and two-line ferrihydrite from homogeneous chemodenitrification reactions between Fe^{2+} and NO_2^- (Table 1). Lepidocrocite, observed as early as 6 h into the reaction (SI Figure 1), catalyzed Fe^{2+} induced reduction of NO_2^- as was found previously.[12,39] Ferrihydrite was also formed within the first 6 h of reaction, albeit at lower concentrations, supporting the previous hypothesis that it also enhances chemodenitrifica-

DOI: 10.1021/es504862x
Environ. Sci. Technol. 2015, 49, 3444−3452

tion.[12,14,43] The high proportions of lepidocrocite and goethite found within the initial time periods are notable because their presence indicates that either those Fe(III) oxides form directly early in the reaction sequence or that ferrihydrite transforms into those minerals prior to being detected.

Despite these different mineral catalysts, chemodenitrification rates were similar in all experimental conditions observed. There was some difference in apparent rate coefficient based on whether NO_2^- (Figure 2C) or Fe^{2+} (Figure 2A) was limiting. This supports our assumption that reaction 1 is operative as our analysis shows second order overall reaction with a dependence on the concentrations of both initial reactants. One of our experiments resulted in lepidocrocite and goethite and another produced nearly equal proportions of lepidocrocite, goethite, and ferrihydrite (Table 1). We hypothesize that the slight variation in mineral phases results from changes in nucleation induced by small changes in initial Fe(III) concentrations and pH generated from Fe^{2+} oxidation. Previous studies on chemodenitrification also found rate variability due to different initial concentrations, mineral catalysts, pH, and the presence of ligands.[13,16,17,39,42,43] We therefore conclude that a range of Fe(III) oxide minerals are produced in homogeneous chemodenitrification and that all of the products generate similar positive feedback in chemodenitrification.

Given the potential ubiquity of N_2O production pathways, characterizing a chemodenitrification signal would help us understand conditions and reactions leading to production of this potent greenhouse gas. The isotopic behavior of NO_2^- and N_2O in chemodenitrification builds upon and complements previous studies.[20,36,44] Cooper et al. (2003) found a $\delta^{15}N$ offset ($\Delta^{15}N = \delta^{15}N_{NO_2^-} - \delta^{15}N_{N_2O}$) of 27 ± 8‰ for their experiment with abiotic NO_3^- reduction. The authors assumed that little to no fractionation occurred during the NO_3^- to NO_2^- reduction step, and thus proposed that $^{15}N_{N_2O}$ was depleted relative to $^{15}N_{NO_2^-}$, as well. Our experiments resulted in a similar $\delta^{15}N$ offset of 28.1 ± 11.0‰ between NO_2^- and N_2O for the excess Fe condition and 27 ± 4.5‰ for the equimolar condition. A more recent study reported $\delta^{15}N$ fractionation ranging between −0.8‰ and 3.4‰ for abiotic N_2O production experiments containing NO_2^-, Fe^{2+}, Fe^{3+}, and NH_2OH substrates.[45] However, a difference in substrates and associated reaction mechanisms likely explains differences in observed $\delta^{15}N$ values.

We measured N_2O SP, the difference in $\delta^{15}N$ between the central (N^α) and outer (N^β) positions of the linear N_2O molecule, because it is thought to reflect the production mechanism.[22] We found that SP values during the course of the experiments ranged from 10‰ to 22‰ during NO_2^- reduction by Fe^{2+}, whereas the SP value from a previous abiotic NO_2^- reduction experiment was −13.3‰.[20] One possible reason for the difference in SP values measured here versus those found by Samarkin et al. (2010) could be a difference in reaction conditions, such as the solute chemistry or contact time between NO_2^- and the mineral catalyst. On the other hand, Heil et al. (2014) found SP values of 34 to 35‰ during abiotic N_2O production experiments with Fe and a NH_2OH/NO_2^- mixture. Toyoda et al. (2005) found SP values of 28.4‰ to 32.2‰ for N_2O produced by abiotic NO_2^- reduction with $(CH_3)_3NBH_3$. The variety of SP values among different studies could be explained by differences in mechanisms associated with different substrates and reaction conditions such as oxidizing vs reducing conditions or different reducing agents. A second possible explanation is an offset in measurement calibration between the laboratories. However, a recent intercalibration by Mohn et al. (2014) found that SP values of reference gases varied by 10‰ between different laboratories, which does not explain the full range of measured SP values.

The SP values observed here (10−22 ‰) fall within the range of end-member SP values for biological N_2O production which are between +38‰ and −10‰ for nitrification, nitrifier-denitrification and denitrification.[24,34,46] Indeed, Peters et al. (2014) found similar N_2O SP values of 0−22 ‰ in soils of the McMurdo Dry Valleys, Antarctica, an environment believed to be suitable for chemodenitrification. Although a $\delta^{15}N$, $\delta^{18}O$ or SP measurement of N_2O alone may not constrain the source of N_2O in natural environments, these results may be used together with other chemical and isotopic measurements to distinguish mechanisms of N_2O production. The co-occurrence of Fe^{2+}, Fe(III) oxides, and NO_2^- combined with SP and isotopic composition of sources and products, could further constrain N cycling and N_2O production reactions in soil and sediment.

Abiotic reactions are considered to be a significant source of atmospheric N_2O, which means that understanding their contribution will support GHG management.[2] Nitrite is not the only type of nitrogen that can be reduced by Fe^{2+}. Ferrous iron reduction of NO_3^-, which is a more widespread anion in soils, may follow similar mechanisms resulting in Fe(III) oxides.[21,42,47] This study presents a suite of measurements that could be used in future work to examine NO_3^- as a starting reactant. Field systems pose a challenge in identifying the reactions consuming NO_x^- and producing N_2O because of their complexity.[20,9,48,49] Taken together, the presence of Fe^{2+}, Fe(III) oxides, and NO_2^- in an anoxic or fluctuating redox environment combined with SP and isotopic composition of sources and products, could be used to indicate possible chemodenitrification in the field. The consistent positive feedback effect of reactive Fe(III) oxide minerals such as goethite, lepidocrocite, and ferrihydrite means that chemodenitrification is possible, and perhaps likely, to occur in environments where NO_x^-, Fe^{2+}, and those minerals coexist.

■ ASSOCIATED CONTENT

Supporting Information

Detailed method information on synchrotron-based analysis, Raleigh calculations, and abiotic oxygen isotope equilibration is included. Also included are complete data on SP, nitrogen isotope effect, and oxygen isotope effect, XRD and EXAFS spectra, and Raleigh plots. This material is available free of charge via the Internet at http://pubs.acs.org/

■ AUTHOR INFORMATION

Corresponding Author

*Phone: (650) 723-5238; e-mail: fendorf@stanford.edu.

Notes

The authors declare no competing financial interest.

■ ACKNOWLEDGMENTS

This research was supported in part by the by the SLAC SFA research program (SLAC FWP 10094), which is funded by the U.S. Department of Energy (DOE) Subsurface Biogeochemical Research (SBR) program within the Office of Biological and Environmental Research. Stanford University School of Earth

DOI: 10.1021/es504862x
Environ. Sci. Technol. 2015, 49, 3444−3452

Sciences and NASA award number NNX11AG45G supported B.P. and K.L.C. Thanks are due to Jessica Lee and Michael Massey for laboratory and design contributions, and three anonymous reviewers for their constructive and thoughtful comments.

REFERENCES

(1) Forster, P.; Ramaswamy, V.; Artaxo, P.; Berntsen, T.; Betts, R.; Fahey, D. W.; Haywood, J.; Lean, J.; Lowe, D. C.; Myhre, G.; et al. Changes in atmospheric constituents and in radiative forcing. In *Climate Change 2007: The Physical Science Basis. Contribution of the Working Group I to the Fourth Assessment Report of the Intergovernmental Panel on Climate Change*.; Solomon, S., Qin, D., Manning, M., Chen, Z., Marquis, M., Averyt, K. B., Tignor, M.; Miller, H. L., Eds.; Cambridge University Press: Cambridge, 2007; pp 131−217.

(2) Ravishankara, A. R.; Daniel, J. S.; Portmann, R. W. Nitrous oxide (N_2O): The dominant ozone-depleting substance emitted in the 21st century. *Science (80)* **2009**, *326*, 123−125 DOI: 10.1126/science.1176985.

(3) Knowles, R. Denitrification. *Microbiol. Mol. Biol. Rev.* **1982**, *46*, 43−70.

(4) Betlach, M. R.; Tiedje, J. M. Kinetic explanation for accumulation of nitrite, nitric oxide, and nitrous oxide during bacterial denitrification. *Appl. Environ. Microbiol.* **1981**, *42*, 1074−1084.

(5) Khalil, M.; Rasmussen, R. The global sources of nitrous oxide. *J. Geophys. Res.* **1992**, *97*, 14,651−14,660.

(6) Spalding, R. F.; Exner, M. E. Occurrence of nitrate in groundwater—A review. *J. Environ. Qual.* **1993**, *22*, 392 DOI: 10.2134/jeq1993.00472425002200030002x.

(7) Philips, S.; Laanbroek, H. J.; Verstraete, W. Origin, causes and effects of increased nitrite concentrations in aquatic environments. *Rev. Environ. Sci. Bio/Technology* **2002**, *1*, 115−141 DOI: 10.1023/A:1020892826575.

(8) Van Cleemput, O.; Samater, A. Nitrite in soils: Accumulation and role in the formation of gaseous N compounds. *Fertil. Res.* **1996**, *45*, 81−89.

(9) Picardal, F. Abiotic and microbial interactions during anaerobic transformations of Fe(II) and NO_x^-. *Front. Microbiol.* **2012**, *3*, 112 DOI: 10.3389/fmicb.2012.00112.

(10) Wullstein, L.; Gilmour, C. Non-enzymatic formation of nitrogen gas. *Nature* **1966**, *210*, 1150−1151.

(11) Kampschreur, M. J.; Kleerebezem, R.; de Vet, W. W. J. M.; van Loosdrecht, M. C. M. Reduced iron induced nitric oxide and nitrous oxide emission. *Water Res.* **2011**, *45*, 5945−5952 DOI: 10.1016/j.watres.2011.08.056.

(12) Tai, Y.-L.; Dempsey, B. A. Nitrite reduction with hydrous ferric oxide and Fe(II): Stoichiometry, rate, and mechanism. *Water Res.* **2009**, *43*, 546−552 DOI: 10.1016/j.watres.2008.10.055.

(13) Coby, A. J.; Picardal, F. W.; Fe, C. S. Inhibition of NO_3^- and NO_2^- reduction by microbial Fe(III) reduction: Evidence of a reaction between NO_2^- and cell surface-bound Fe^{2+}. *Appl. Environ. Microbiol.* **2005**, *71* DOI 10.1128/AEM.71.9.5267.

(14) Van Cleemput, O.; Baert, L. Nitrite stability influenced by iron compounds. *Soil Biol. Biochem.* **1983**, *15*, 137−140.

(15) Guerbois, D.; Ona-nguema, G.; Morin, G.; Abdelmoula, M.; Laverman, A. M.; Mouchel, J.; Barthelemy, K.; Maillot, F.; Brest, J. Nitrite reduction by biogenic hydroxycarbonate green rusts: Evidence for hydroxy-nitrite green rust formation as an intermediate reaction product. *Environ. Sci. Technol.* **2014**, *48*, 4505−4514.

(16) Williams, A. G. B.; Scherer, M. M. Spectroscopic evidence for Fe(II)-Fe(III) electron transfer at the iron oxide-water interface. *Environ. Sci. Technol.* **2004**, *38*, 4782−4790.

(17) Sorensen, J.; Thorling, L. Stimulation by lepidocrocite of Fe(II)-dependent nitrite reduction. *Geochim. Cosmochim. Acta* **1991**, *55*, 1289−1294.

(18) Matocha, C. J.; Dhakal, P.; Pyzola, S. M. The role of abiotic and coupled biotic/abiotic mineral controlled redox processes in nitrate reduction. In *Advances in Agronomy Vol. 115*, Advances in Agronomy; Sparks, D. L., Ed.; Elsevier, 2012; Vol. *115*, pp 181−214.

(19) Venterea, R. T. Nitrite-driven nitrous oxide production under aerobic soil conditions: Kinetics and biochemical controls. *Glob. Chang. Biol.* **2007**, *13*, 1798−1809 DOI: 10.1111/j.1365-2486.2007.01389.x.

(20) Samarkin, V. A.; Madigan, M. T.; Bowles, M. W.; Casciotti, K. L.; Priscu, J. C.; Mckay, C. P.; Joye, S. B. Abiotic nitrous oxide emission from the hypersaline Don Juan Pond in Antarctica. *Nat. Geosci.* **2010**, *3*, 341−344 DOI: 10.1038/NGEO847.

(21) Ernstsen, V.; Binnerup, S. J.; Sorensen, J. Reduction of nitrate in clayey subsoils controlled by geochemical and microbial barriers. *Geomicrobiol. J.* **1998**, *15*, 195−207.

(22) Yoshida, N.; Toyoda, S. Constraining the atmospheric N_2O budget from intramolecular site preference in N_2O isotopomers. *Nature* **2000**, *405*, 330−334 DOI: 10.1038/35012558.

(23) Popp, B. N.; Westley, M. B.; Toyoda, S.; Miwa, T.; Dore, J. E.; Yoshida, N.; Rust, T. M.; Sansone, F. J.; Russ, M. E.; Ostrom, N. E.; et al. Nitrogen and oxygen isotopomeric constraints on the origins and sea-to-air flux of N_2O in the oligotrophic subtropical North Pacific gyre. *Global Biogeochem. Cycles* **2002**, *16* (4), 1064 DOI: 10.1029/2001GB001806.

(24) Toyoda, S.; Mutobe, H.; Yamagishi, H.; Yoshida, N.; Tanji, Y. Fractionation of N_2O isotopomers during production by denitrifier. *Soil Biol. Biochem.* **2005**, *37*, 1535−1545 DOI: 10.1016/j.soilbio.2005.01.009.

(25) Sutka, R. L.; Ostrom, N. E.; Ostrom, P. H.; Gandhi, H.; Breznak, J. A. Nitrogen isotopomer site preference of N_2O produced by *Nitrosomonas europaea* and *Methylococcus capsulatus* Bath. *Rapid Commun. Mass Spectrom.* **2003**, *17*, 738−745 DOI: 10.1002/rcm.968.

(26) Schmidt, H.-L.; Werner, R. A.; Yoshida, N.; Well, R. Is the isotopic composition of nitrous oxide an indicator for its origin from nitrification or denitrification? A theoretical approach from referred data and microbiological and enzyme kinetic aspects. *Rapid Commun. Mass Spectrom.* **2004**, *18*, 2036−2040 DOI: 10.1002/rcm.1586.

(27) Well, R.; Kurganova, I.; Lopes de Gerenyu, V.; Flessa, H. Isotopomer signatures of soil-emitted N_2O under different moisture conditions—A microcosm study with arable loess soil. *Soil Biol. Biochem.* **2006**, *38*, 2923−2933 DOI: 10.1016/j.soilbio.2006.05.003.

(28) Westley, M. B.; Yamagishi, H.; Popp, B. N.; Yoshida, N. Nitrous oxide cycling in the Black Sea inferred from stable isotope and isotopomer distributions. *Deep Sea Res., Part II* **2006**, *53*, 1802−1816 DOI: 10.1016/j.dsr2.2006.03.012.

(29) Viollier, E.; Inglett, P.; Hunter, K.; Roychoudhury, A.; Van Cappellen, P. The ferrozine method revisited: Fe(II)/Fe(III) determination in natural waters. *Appl. Geochem.* **2000**, *15*, 785−790.

(30) Pai, S.; Yang, C.; Riley, J. Formation kinetics of the pink azo dye in the determination of nitrite in natural waters. *Anal. Chim. Acta* **1990**, *232*, 345−349.

(31) McIlvin, M. R.; Altabet, M. A. Chemical conversion of nitrate and nitrite to nitrous oxide for nitrogen and oxygen isotopic analysis in freshwater and seawater. *Anal. Chem.* **2005**, *77*, 5589−5595 DOI: 10.1021/ac050528s.

(32) Casciotti, K. L.; Böhlke, J. K.; McIlvin, M. R.; Mroczkowski, S. J.; Hannon, J. E. Oxygen isotopes in nitrite: Analysis, calibration, and equilibration. *Anal. Chem.* **2007**, *79*, 2427−2436 DOI: 10.1021/ac061598h.

(33) McIlvin, M.; Casciotti, K. Fully automated system for stable isotopic analyses of dissolved nitrous oxide at natural abundance levels. *Limnol. Oceanogr. Methods* **2010**, 54−66 DOI: 10.4319/lom.2010.8.54.

(34) Frame, C. H.; Casciotti, K. L. Biogeochemical controls and isotopic signatures of nitrous oxide production by a marine ammonia-oxidizing bacterium. *Biogeosciences Discuss.* **2010**, *7*, 3019−3059 DOI: 10.5194/bgd-7-3019-2010.

(35) Mohn, J.; Wolf, B.; Toyoda, S.; Lin, C.-T.; Liang, M.-C.; Brüggemann, N.; Wissel, H.; Steiker, A. E.; Dyckmans, J.; Szwec, L.; et al. Interlaboratory assessment of nitrous oxide isotopomer analysis by isotope ratio mass spectrometry and laser spectroscopy: Current

DOI: 10.1021/es504862x
Environ. Sci. Technol. 2015, 49, 3444−3452

status and perspectives. *Rapid Commun. Mass Spectrom.* **2014**, *28*, 1995−2007 DOI: 10.1002/rcm.6982.
(36) Cooper, D.; Picardal, F. W.; Schimmelmann, A.; Coby, A. J. Chemical and biological interactions during nitrate and goethite reduction by *Shewanella putrefaciens* 200. *Appl. Environ. Microbiol.* **2003**, *69*, 3517−3525 DOI: 10.1128/AEM.69.6.3517.
(37) Kopf, S. H.; Henny, C.; Newman, D. K. Ligand-enhanced abiotic iron oxidation and the effects of chemical vs. biological iron cycling in anoxic environments. *Environ. Sci. Technol.* **2013**, *47*, 2602−2611 DOI: 10.1021/es3049459.
(38) Dhakal, P.; Matocha, C.; Huggins, F.; Vandiviere, M. Nitrite reactivity with magnetite. *Environ. Sci. Technol.* **2013**, *47*, 6206−6213 DOI: 10.1021/es304011w.
(39) Rakshit, S.; Matocha, C. J.; Coyne, M. S. Nitrite reduction by siderite. *Soil Sci. Soc. Am. J.* **2008**, *72*, 1070 DOI: 10.2136/sssaj2007.0296.
(40) Buchwald, C.; Casciotti, K. L. Isotopic ratios of nitrite as tracers of the sources and age of oceanic nitrite. *Nat. Geosci.* **2013**, *6*, 308−313 DOI: 10.1038/ngeo1745.
(41) Bryan, B.; Shearer, G.; Skeeters, J.; Kohl, D. Variable expression of the nitrogen isotope effect associated with denitrification of nitrite. *J. Biol. Chem.* **1983**, *258*, 8613−8617.
(42) Postma, D. Kinetics of nitrate reduction by detrital Fe(II)-silicates. *Geochim. Cosmochim. Acta* **1990**, *54*, 903−908.
(43) Hansen, H.; Borggaard, O.; Sorensen, J. Evaluation of the free energy of formation of Fe(II)-Fe(III) hydroxide-sulphate (green rust) and its reduction of nitrite. *Geochim. Cosmochim. Acta* **1994**, *58*, 2599−2608 DOI: 10.1016/0016-7037(94)90131-7.
(44) Peters, B.; Casciotti, K. L.; Samarkin, V. A.; Madigan, M. T.; Schutte, C. A.; Joye, S. B. Stable isotope analyses of NO_2^-, NO_3^-, and N_2O in the hypersaline ponds and soils of the McMurdo Dry Valleys, Antarctica. *Geochim. Cosmochim. Acta* **2014**, *135*, 87−101.
(45) Heil, J.; Wolf, B.; Brüggemann, N. Site-specific ^{15}N isotopic signatures of abiotically produced N_2O. *Geochim. Cosmochim. Acta* **2014**, *139*, 72−82 DOI: 10.1016/j.gca.2014.04.037.
(46) Wunderlin, P.; Lehmann, M. Isotope signatures of N_2O in a mixed microbial population system: Constraints on N_2O producing pathways in wastewater treatment. *Environ. Sci. Technol.* **2013**, *47*, 1339−1348 DOI: 10.1021/es303174x.
(47) Ottley, C. J.; Davison, W.; Edmunds, W. M. Chemical catalysis of nitrate reduction by iron(II). *Geochim. Cosmochim. Acta* **1997**, *61*, 1819−1828 DOI: 10.1016/S0016-7037(97)00058-6.
(48) Ernstsen, V.; Morup, S. Nitrate Reduction in clayey till by iron(II) in clay minerals. *Hyperfine Interact.* **1992**, *70*, 1001−1004.
(49) Venterea, R. T.; Rolston, D. Nitric and nitrous oxide emissions following fertilizer application to agricultural soil: Biotic and abiotic efforts. *J. Geophys. Res.* **2000**, *105* DOI: 10.1029/2000JD900025.

■ NOTE ADDED AFTER ASAP PUBLICATION

This paper was originally published ASAP on February 26, 2015. Several text errors were discovered, and the presentation of O-NO_2 needed to be modified. The corrected version was published on March 2, 2015.

DOI: 10.1021/es504862x
Environ. Sci. Technol. 2015, 49, 3444−3452